OPEN ACCESS
JOURNAL OF ADVANCED DIELECTRICS
Vol. 11, No. 3 (2021) 2140007 (6 pages)
© The Author(s)
DOI: 10.1142/S2010135X21400075

XI'AN JIAOTONG UNIVERSITY

World Scientific
www.worldscientific.com

Effects of crystallization kinetics on the dielectric and electrical properties of $BiFeO_3$ films

Y. González-Abreu[*,†], S. P. Reis[‡], F. E. Freitas[*,§], J. A. Eiras[¶] and E. B. Araújo[*,||]

[*]*Department of Physics and Chemistry*
São Paulo State University, 15385-000 Ilha Solteira, Brazil

[†]*Facultad de Física, Universidad de La Habana. San Lázaro y L*
Vedado. La Habana 10400, Cuba

[‡]*Federal Institute of Education, Science and Technology of São Paulo*
15503-110 Votuporanga, Brazil

[§]*University of Rio Verde (UniRV), 75901-970 Rio Verde, Brazil*

[¶]*Departamento de Física, Grupo de Materiais Ferróicos*
Universidade Federal de São Carlos, São Carlos, Brazil

[||]eudes.borges@unesp.br

Received 25 February 2021; Revised 24 April 2021; Accepted 20 May 2021; Published 16 June 2021

$BiFeO_3$ thin films were prepared using the chemical solution route on $Pt/TiO_2/SiO_2/Si(100)$ substrates under different crystallization kinetics. The crystallization kinetic effects on the dielectric and electrical properties have been investigated. These properties included dielectric permittivity, electric modulus, electrical conductivity measurements as a function of the temperature (300–525 K) and frequency (10^2–10^6 Hz), and leakage current measurements electric field range ±30 kV/cm at room temperature. The differences observed in conductivity and current density of the $BiFeO_3$ films were discussed in terms of possible defects induced by the crystallization kinetic. An anomalous relaxor-like dielectric behavior characterized by a broad maximum in the real dielectric permittivity as a function of temperature and the low-frequency dielectric dispersion has been observed. The nonexpected peaks in the real permittivity were accompanied by increasing at least four orders in the conductivity's magnitude at high temperatures. The origin of the relaxor-like dielectric anomalies is discussed, suggesting that the dielectric permittivity peaks are artifacts due to carrier migration correlated to the onset of the Maxwell–Wagner effect.

Keywords: $BiFeO_3$; thin films; dielectric relaxation; leakage current.

1. Introduction

The bismuth ferrite $BiFeO_3$ (BFO) is one of the most studied multiferroics, with a Neel temperature of 643K and a ferroelectric-paraelectric phase transition 1103 K.[1–4] The large remnant polarization of BFO[5–7] turns it suitable for practical applications as a lead-free material. BFO thin films are useful for the development of memories, spintronic devices and resistive switching devices.[8,9] Furthermore, BFO is of interest to the scientific community due to its potential photovoltaic effect, with a bandgap between 2.6 eV and 3.0 eV, lower than other ferroelectric materials.[10,11]

The presence of defects in the BFO has an intrinsic relationship with the sample preparation conditions.[12–14] Theoretical studies have modeled the formation and association of single point defects in the material such as polarons, cation vacancies (bismuth/iron) and oxygen vacancies. The role of single vacancies in the generation of states localized within the forbidden band and the behavior of the iron vacancies carrying an electric dipole are supported.[15] Interactions between point defects that form complex bismuth/iron-oxygen vacancies defects are also considered.[15,16] The high leakage current in BFO samples has been mainly related to Fe^{2+} ions and oxygen vacancies, with a more significant contribution from oxygen vacancies than Fe^{2+} and can even behave as complex defects.[17–19] Leakage current studies in BFO thin films have been reported with the validation of various mechanisms as space charge limited current (SCLC), Poole–Frenkel emission and interface-limited Schottky emission.[17–20]

Dielectric studies in hot-pressed BFO ceramics reported an analogous response to materials with a giant dielectric permittivity and a step behavior.[21] The authors found three relaxation processes at the studied temperature range as a combination of electronic charge carriers hopping, at low temperatures, grain boundary effects, and secondary phase

[||]Corresponding author.

This is an Open Access article published by World Scientific Publishing Company. It is distributed under the terms of the Creative Commons Attribution 4.0 (CC BY) License which permits use, distribution and reproduction in any medium, provided the original work is properly cited.

acting like an internal barrier layer, for medium temperatures and the short-range hopping of oxygen vacancies at higher temperatures. They suggested the possibility of improving the dielectric parameters from mechanochemical synthesis and thermal treatments.[21] Further, Ke *et al*.[22] tuned the concentration of oxygen vacancies and the amount of Fe^{2+} in BFO ceramics with a direct effect on the samples' dielectric and ferroelectric properties. A transition from high resistive to low resistive is manifested from the increase in the concentration of Fe^{2+} (oxygen vacancies) in the samples. The relaxation process due to the contribution of the grain was related to a polaronic effect, while the contribution of the grain boundary to relaxation showed higher activation energy around 0.61 eV.

The effects of the grain boundaries are determinants for the electrical response of BFO. Also, the design of the films and the crystallization conditions could influence their properties. This work aims to study the dielectric and electric properties of $BiFeO_3$ thin films prepared under different crystallization conditions. The variations in the films' grain and grain boundary contributions are evaluated from the complex electrical modulus response. The study of the conductivity and leakage current mechanisms is presented from bulk-limited current mechanisms.

2. Experimental Procedure

The $BiFeO_3$ thin films studied in this work were obtained by chemical acetate solution route from the dissolution of $Bi(NO_3)_3 \cdot 5H_2O$ (Sigma-Aldrich 99.9%) and iron nitrate nonahydrate $Fe(NO_3)_3 \cdot 9H_2O$ (Sigma-Aldrich 99.9%) into glacial acetic acid (Sigma-Aldrich 99.9%) at 57 °C, under stirring for 10 min, and finalized at 80 °C for 30 min. The final solution was used to prepare two different BFO thin films on $Pt/TiO_2/SiO_2/Si(100)$ substrates by spin coating at 5000 rpm for 30 s. The samples were prepared in air atmosphere in three steps: (i) 4 depositions with the organic evaporation at ~250 °C for 5 min, followed by the crystallization; (ii) repeat the previous step with three depositions, and (iii) repeat the previous step with three depositions followed by a final crystallization. The first BFO film (BFO-RH) was crystallized at 600 °C for 30 min by rapid heating (RH), introducing the film directly into an electric furnace at 600 °C. In contrast, the second BFO film (BFO-SH) was crystallized at 600 °C for 30 min by slow heating (SH), heating the sample from 300 °C to 600 °C at 5 °C/min. After crystallization, it was cooled to 300 °C. The final films were ~ 500-nm thick.

The BFO films' structure was investigated by X-ray diffraction (XRD) technique, using a Rigaku Ultima IV diffractometer with CuK_α radiation at room temperature. The morphology and composition were studied by scanning electron microscopy (SEM) using a Carl Zeiss EVO microscope. For the electrical measurements, circular gold electrodes of 300 μm in diameter were sputtered onto the films to form metal/ferroelectric/metal capacitors. An Agilent 4284A LCR meter was used for the dielectric measurements in the temperature and frequency ranges 300–530 K and 1 kHz–1 MHz. *I–V* characteristic was obtained at room temperature using a Keithley 6517B electrometer with a maximal electric field of 30 kV/cm and an increasing rate of 0.4 kV/cm.

3. Results and Discussion

The rhombohedral structure *R3c* of the studied BFO films, with $a = b = 5.55(5)$ Å and $c = 13.8(6)$ Å, was confirmed from XRD analysis (not shown here). The lattice parameters are in good agreement with previous studies in the literature reported for the bismuth ferrite.[23]

Figures 1(a) and 1(b) show the SEM images for both BFO-RH and BFO-SH films, respectively. The microstructure of the BFO-SH exhibits grains with high definition and well-defined grain boundaries, with an average grain size of 137 ± 40 nm, while grain size of 121 ± 30 nm, with grain and grain boundary structures not well-defined, were obtained for the BFO-RH film. The pores size is more prominent in BFO-SH film (50–240 nm) than in BFO-RH (50–130 nm) due to the variation in the crystallization condition for the films. These holes could influence the dielectric behavior reducing the dielectric permittivity values. For the studied films, the real dielectric permittivity at 1 MHz is higher in BFO-RH than BFO-SH in correspondence with the porosity of the samples.

Figures 2(a) and 2(b) show the real part of the dielectric permittivity (ε') as a function of temperature for the BFO-RH and BFO-SH films, respectively, at different frequencies. The temperature dependence of the imaginary part of the dielectric permittivity (ε'') of both films was shown in Figs. 2(c) and 2(d) at the same frequencies. At room temperature, both films' real permittivity is almost frequency independent in the studied frequency range, such that the observed permittivity ranges from 229 to 196 for the BFO-RH film and from 166 to 145 for the BFO-SH film. These values indicate that the permittivity decreases ~ 14 % from 1 kHz to 1 MHz for both films.

The dielectric permittivity values in the present work at room temperature agree with values reported in the literature

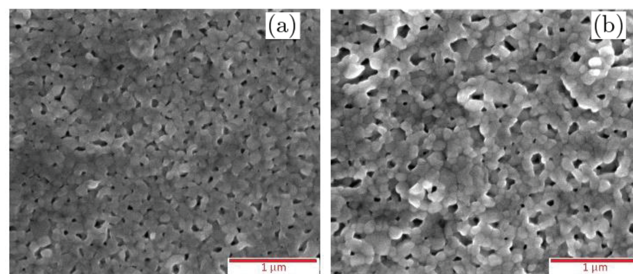

Fig. 1. SEM images of the (a) BFO-RH and (b) BFO-SH thin films at room temperature.

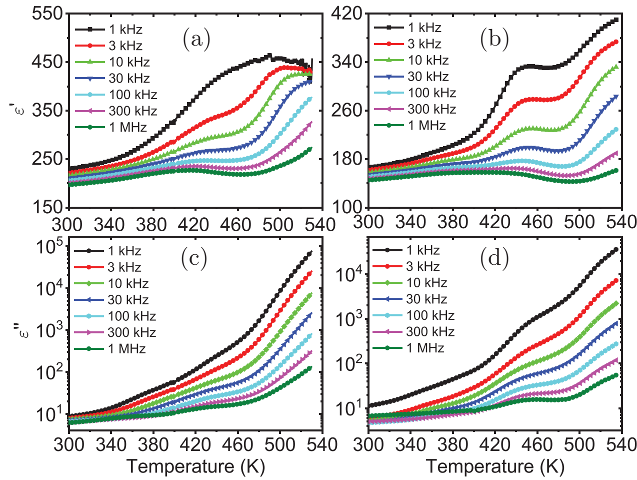

Fig. 2. Real part of the dielectric permittivity (ε') as a function of the temperature of the (a) BFO-RH and (b) BFO-SH thin films at selected frequencies. Temperature dependence of the imaginary part of the dielectric permittivity (ε'') of the (c) BFO-RH and (d) BFO-SH films at the same frequencies.

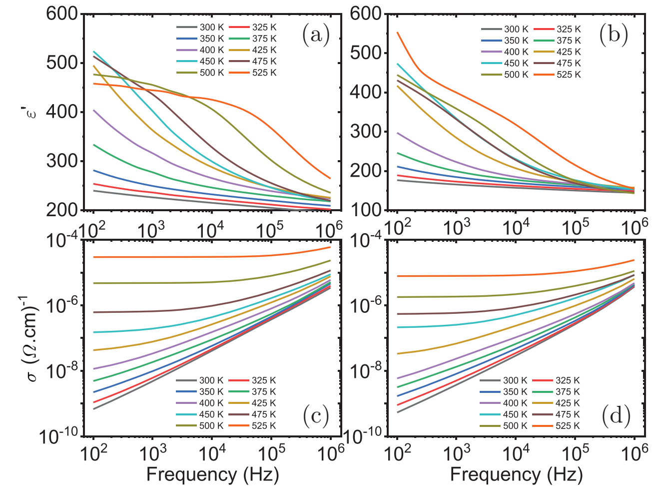

Fig. 3. Frequency dependency of the real part of the dielectric permittivity (ε') of (a) BFO-RH and (b) BFO-SH thin films at selected temperatures. AC conductivity as a function of the frequency of the (c) BFO-RH and (d) BFO-SH films at the same temperature range in (a) and (b).

for BFO thin films prepared by similar chemical routes.[24] On the other hand, increasing the temperature, an anomalous dielectric permittivity behavior was observed. Noticeable high-frequency dispersion of dielectric permittivity was observed with broad peaks around 480 K and 440 K in Figs. 2(a) and 2(b) shifting to higher temperatures and frequencies. The peaks observed in the real permittivity were accompanied by an increase of at least four orders in the magnitude of imaginary permittivity at high temperatures, as observed in Figs. 2(c) and 2(d). Since $\varepsilon'' \propto \sigma(\omega)$, the observed increase in the imaginary dielectric permittivity indicates an extrinsic contribution of the conductivity at high temperatures in the studied BFO films.

With a well-known high Curie temperature, the dielectric permittivity peaks of $BiFeO_3$ in Figs. 2(a) and 2(b) cannot be due to the ferroelectric transitions in this multiferroic. In addition, the observed relaxor-like dielectric behavior is most probably associated with artifacts of carrier migration across interfaces in BFO films since the $BiFeO_3$ is not a ferroelectric relaxor material. Careful frequency dependence of dielectric permittivity was carried out to examine the observed unusual relaxor-like dielectric behavior's possible origins.

Figures 3(a) and 3(b) show the real dielectric permittivity as a function of frequency for the BFO-RH and BFO-SH thin films, respectively, at selected temperatures in the range 300–525 K. No significative frequency dispersions were observed in the dielectric permittivity for both BFO films at 300 K. However, when the temperature increases a pronounced dielectric permittivity increasing was observed at frequencies below 100 kHz, leading to a permittivity plateau around $\varepsilon' \sim 470$ below this frequency for the BFO-RH film at 525 K, as shown in Fig. 3(a). In contrast, no plateau is observed and the dielectric permittivity increases continuously in BFO-SH at frequencies lower than 100 kHz within the same temperature range, as observed in Fig. 3(b).

The *ac* conductivity as a function of the frequency of the BFO-RH and BFO-SH films were shown in Figs. 3(c) and 3(d) at the same temperature range in Figs. 3(a) and 3(b). The frequency dependence of the conductivity can be described by the Jonscher power-law relation $\sigma(\omega) = \sigma_{dc} + A\omega^n$, where σ_{dc} is the frequency-independent *dc* conductivity, the exponent n and the coefficient A are parameters dependent on temperature and material ($0 < n < 1$), and $A\omega^n$ represents the dielectric dispersion.[25] The log–log $\sigma(\omega)$ curves in Fig. 3(c) and 3(d) are flattened in the low-frequency region at 300 K. Increasing the temperature, the flattened region becomes wider and is shifted toward higher frequencies, and the conductivity becomes almost frequency-independent. This frequency-independent plateau-like region observed in the low-frequency regime is associated with the conductivity σ_{dc}. So, at 525 K the conductivity σ_{dc} of both BFO films is dominant over almost all frequencies in the studied range.

In Fig. 3, the increase in real (ε') and imaginary (ε'') dielectric permittivity ($\varepsilon'' \propto \sigma$) shown at lower frequencies at temperatures higher than 425 K can be associated with the influence of the electrical conductivity over the dielectric response. Also, ε' is characterized by the steps. These steps are clear at mid and low frequencies, increasing the size with the temperature and decreasing frequency. The dielectric behavior could be seen as combining several relaxation processes in the studied BFO thin films. The shape of $\varepsilon'(\omega)$ curve in Fig. 3(a) at 525 K is evidence of the Maxwell-Wagner (MW) effect due to the space charge on the interfaces. In nonferroelectric materials, the MW effect signature is often associated with a frequency-independent plateau in $\sigma(\omega)$ curves at frequencies below 100 kHz, indicating a dominance of the *dc*

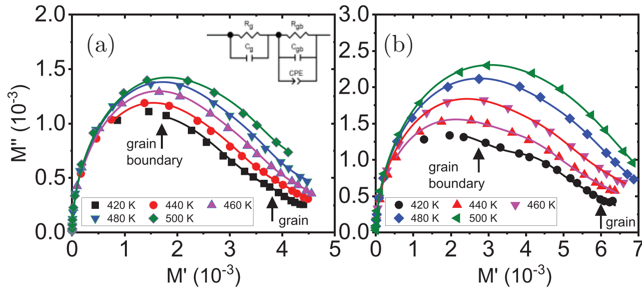

Fig. 4. Nyquist plots (M'' versus M') of (a) BFO-RH and (b) BFO-SH thin films at different temperatures. Symbols are experimental data while lines are theoretical fits obtained from the equivalent circuit shown in (a).

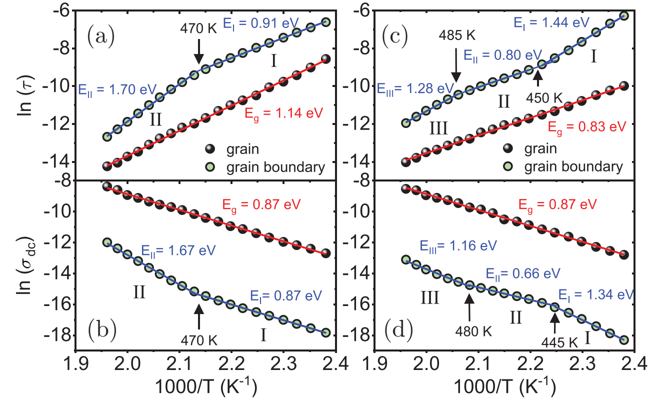

Fig. 5. Plots of (a) ln(τ) and (b) ln(σ_{dc}) of grain and grain boundary as a function of reciprocal temperature for the BFO-RH film. Similar plots are shown in (c) and (d) for the BFO-SH film. Lines are linear fittings.

conductivity and a lack of hopping charge carrier polarization at low frequency.[26] The plateau-like region in Figs. 3(c) and 3(d) in the mentioned frequency range and above 425 K indicates that the space charge mechanisms dominate the dielectric behavior observed in the present work. The MW effect is more pronounced in the BFO-RH film than BFO-SH because the rapid heating induces more defects at interfaces than SH to the crystallization. Also, the plot of the impedance (Z') against (Z''/f) at different temperatures is suitable to indicate that the electrode effects. In the present work, these effects are pronounced at temperatures above 425 K. Based on the above discussion, there is strong evidence that the relaxor-like dielectric behavior in Figs. 2(a) and 2(b) is correlated to the onset of MW effect, confirming that $\varepsilon'(T)$ peaks are artifacts due to carrier migration.

Figure 4 shows the complex electric modulus Nyquist plots of M'' versus M' of the BFO films at different temperatures from 420 K to 500 K. In Figs. 4(a) and 4(b), the shoulder around 420 K suggests the overlap of grain and grain boundaries contributions, with better resolution for BFO-SH than for BFO-RH film. The equivalent circuit inserted in Fig. 4(a) represents the studied BFO films' electrical response. C_{gb}, R_{gb}, C_g, R_g elements are the capacitive and resistive components associated with the grain and grain boundary. The CPE element reflects the existence of a relaxation time distribution related to grain boundaries. In Fig. 4, lines are theoretical fits obtained from the model to obtain the relaxation time (τ) and *dc* conductivity (ε_{dc}) for the grain and grain boundary.

The relaxation time (τ) and *dc* conductivity (σ_{dc}) are thermally activated processes described by the Arrhenius relations $\tau = \tau_0 \exp(E_\tau/k_BT)$ and $\sigma_{dc} = \sigma_0 \exp(-E_{dc}/k_BT)$, where is the Boltzmann constant, and are the activation energies, while τ_0 and σ_0 are pre-exponential factors. Figures 5(a) and 5(b) show, respectively, the ln(τ) and ln(σ_{dc}) as a function of reciprocal temperature, similar plots are shown in Figs. 5(c) and 5(d) for BFO-SH film. The activation energies E_τ and E_{dc} were obtained from linear fits, indicated in Fig. 5 for grain and grain boundary.

The contributions of the grain to the relaxation and dc conductivity are characterized by one thermally activated process in the temperature range 420–510 K. For the BFO-SH film, the activation energies from the relaxation time and dc conductivity of grain show essentially the same value around 0.83 eV, indicating the same process, while different values observed for the BFO-RH film (0.87 versus 1.14 eV) suggest that dc conductivity processes prevail over relaxation processes. The main differences between the BFO films come from the behavior of the grain boundaries as can be seen in Fig. 5. The grain boundary for BFO-RH film presents two activation energy regions delimited around 470 K for τ and σ_{dc}, though BFO-SH presents three regions from the change in slopes around 450 K and 480 K. The proximity between the activation energy values for the relaxation time and the dc conductivity of the grain boundary suggests that both processes have the same origin. However, the activation energy values are different between the samples.

Relaxation processes at temperatures of 220 K and 570 K in BFO bulk ceramics, with similar dielectric behavior characterized by steps, have been related to Fe^{2+}/Fe^{3+} carrier hopping processes (220–370 K) with activation energy values around 0.4 eV. For temperatures between 370 K and 570 K were related to the grain boundary and the second phase (370–470 K) and the short-range hopping of the oxygen vacancies (above 470 K) resembles dipole reorientation.[21] In the present work, the activation energy values related to the relaxation and dc processes in the grain (0.83–1.14 eV) are higher than those reported for the Fe^{2+}/Fe^{3+} carrier hopping. These processes are also evidenced at higher temperature range, suggesting that they could originate from the ionized oxygen vacancies.[21,27,28] The higher resistive behavior and the activation energies for the grain boundary advise about a blocking effect acting as insulating barriers between conductive grains. This blocking effect could originate from the chemical inhomogeneity between grain and grain boundaries, with space

charge accumulation (Maxwell–Wagner effect). Mobility through grain boundaries could be affected by depletion layer zones with the influence of the localized potential barrier (Φ), leading to higher activation energy values.[29,30] Therefore, the dielectric behavior of BFO films is mainly related to grain boundaries effects. From SEM images the differences in the grain and grain boundary structures of the films due to the modification in the crystallization conditions were shown. The study presented above showed that this microstructural variation influences the relaxation and dc conductivity processes due to the grain boundary, improving these processes in BFO-SH film. Two activation energy value regions evidence this for BFO-RH and three for BFO-SH film. Furthermore, for BFO-RH the differences in the activation energy values for the grain and grain boundary increase above 470 K for both processes, whereas for BFO-SH the differences are evidenced from low temperatures in the studied temperature range (420–510 K). Suppose the higher activation energy values for the grain boundary contribution are related to blocking effects due to the chemical inhomogeneity between grain and grain boundary. In that case, this inhomogeneity is enhanced for the BFO-SH due to SH during the crystallization. It can be concluded that the differences in the dielectric behavior of the films for temperatures from 420 K to 510 K are originated from the changes in the grain boundary response as a consequence of the crystallization conditions.

Figure 6(a) shows the leakage current density as a function of the electric field of both BFO-RH and BFO-SH films. The J–E curves were recorded, increasing the electric field from −30 kV/cm to +30 kV/cm (up) and decreasing from +30 kV/cm to −30 kV/cm (down). The BFO-SH film exhibits a correspondence between up and down measurements. Still, a hysteresis due to the rapid decrease of $J(E)$ was observed in Fig. 6(a) for BFO-RH film, leading to a minimum J value of before zero electric field. The BFO-SH presents higher leakage current density values than BFO-RH, and their conductivities at room temperature and at 10 kV/cm were 4.4×10^{-10} and 5.2×10^{-12} Ω^{-1}cm^{-1}, respectively.

Figure 6(b) shows the study of the conduction mechanisms based on $\log(J)$ versus $\log(E)$ plots of BFO-RH and BFO-SH films at room temperature for the positive (+E) and negative (−E) field. The transition from a linear Ohmic ($J \propto E$) relationship to a SCLC mechanism ($J \propto E^2$) is evidenced by changes in slopes in BFO-SH curves. The SCLC mechanism (above 7.6 kV/cm) is verified when the injected charge carriers from the electrode exceeded the thermally excited ones, which are bulk-limited conduction mechanisms.[17,20] On the other hand, the Ohmic behavior is not verified for BFO-RH at the same electric field range. The linear dependence $J \propto E$ is evidenced for $+E$ near 20 kV/cm, whereas for −E it is not exhibited this linear dependence for the studied E-field range, which is indicative of differences in the generated free-carrier density for the films. It is supported that the SCLC model is presented in ferroelectrics materials with deep traps.[31] The $\log(J)$ versus $\log(E)$ plots exhibit first an ohmic behavior at low field ($J \propto E$) due to the predominance of the thermally generated carriers. For higher fields, the injected carriers fill the traps and a trap-filled-limited (TFL) region could be evidenced with a relationship of $J \propto E^n$ ($n > 2$). From Fig. 6(b), in the BFO-SH film, the SCLC mechanism above 7.6 kV/cm presents a higher slope for −E than for +E which could be related to differences in the trap-filling from the inversion of the electric field.

The studies in BFO materials have demonstrated that oxygen vacancy generation increases the current density rather than Fe^{2+}.[17–20] The high current density for BFO-SH could result from a higher oxygen vacancy concentration, which favors the free charge mobility from the generation of deep trap levels in the bandgap. However, the effects of Fe^{2+}/Fe^{3+} should be considered from the field-assisted conduction due to the electronic transfers between Fe^{2+} and Fe^{3+} where Fe^{2+} is virtually hopping among neighbor positions.[17] Also, it is supported that leakage current could be improved due to variations in the growth conditions in BFO films that influence the structural defects, and the structural inhomogeneities related to the porosity could trap oxygen vacancies.[32] For the BFO-SH, the SEM image reveals a higher porosity which could contribute to the leakage current increase. The obtained result in the present work confirms the effect of the annealing conditions on the leakage current behavior.

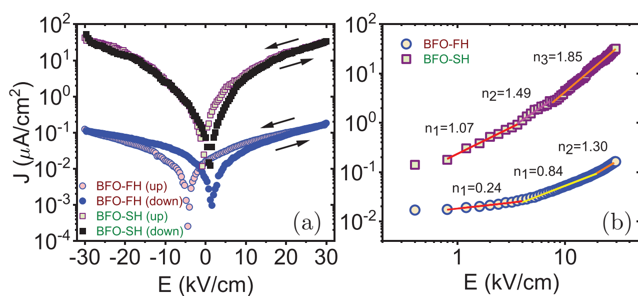

Fig. 6. (a) Current density (J) as a function of electric field (E) and (b) logarithmic plot of current density as a function of logarithmic electric field of BFO-RH and BFO-SH films at room temperature.

4. Conclusions

In summary, the dielectric behavior and leakage current mechanisms of $BiFeO_3$ films with different thermal histories were studied. The grain and grain boundary contributions were analyzed using electric modulus spectroscopy with an essential difference in the thermally activated relaxation and dc conductivity processes. The obtained activation energies for the grain (0.83–1.14 eV) suggest that oxygen vacancies probably dominate the studied films' conduction mechanism. In contrast, the grain boundaries activation values suggest blocking effects, originated from the chemical inhomogeneity between grain and grain boundary and enhanced, for the BFO-SH film, with the heating conditions during the

crystallization. The linear Ohmic conductivity is considered from the leakage current study in the samples, whereas an SCLC mechanism is evidenced in slowly heated BFO-SH film above 7.6 kV/cm. The higher leakage current in BFO film slowly heated up to the crystallization (BFO-SH) could be related to high free charge mobility than for BFO film rapid heated to the crystallization (BFO-RH).

Acknowledgments

This research was supported by the Fundação de Amparo à Pesquisa do Estado de São Paulo — FAPESP (Project: 2017/13769-1) and Coordenação de Aperfeiçoamento de Pessoal de Nível Superior — CAPES (CAPES-PRINT Project: 88881.310513/2018-01, 88887.469068/2019-00 and 88887.508251/2020-00).

References

[1] J. Wang, J. B. Neaton, H. Zheng, V. Nagarajan, S. B. Ogale, B. Liu, D. Viehland, V. Vaithyanathan, D. G. Schlom, U. V. Waghmare, N. A. Spaldin, K. M. Rabe, M. Wuttig and R. Ramesh, Epitaxial $BiFeO_3$ multiferroic thin film heterostructures, *Science* **299**, 1719 (2003).

[2] G. Catalan and J. F. Scott, Physics and applications of bismuth ferrite, *Adv. Mater.* **21**, 2463 (2009).

[3] T. Zhao, A. Scholl, F. Zavaliche, K. Lee, M. Barry, A. Doran, M. P. Cruz, Y. H. Chu, C. Ederer, N. A. Spaldin, R. R. Das, D. M. Kim, S. H. Baek, C. B. Eom and R. Ramesh, Electrical control of antiferromagnetic domains in multiferroic $BiFeO_3$ films at room temperature, *Nat. Mater.* **5**, 823 (2006).

[4] J. B. Neaton, C. Ederer, U. V. Waghmare, N. A. Spaldin and K. M. Rabe, First-principles study of spontaneous polarization in multiferroic $BiFeO_3$, *Phys. Rev. B* **71**, 014113 (2005).

[5] D. Sando, A. Barthélémy and M. Bibes, $BiFeO_3$ epitaxial thin films and devices: Past, present and future, *J. Phys.: Condens. Matter* **26**, 473201 (2014).

[6] D. Lebeugle, D. Colson, A. Forget and M. Viret, Very large spontaneous electric polarization in $BiFeO_3$ single crystals at room temperature and its evolution under cycling fields, *Appl. Phys. Lett.* **91**, 022907 (2007).

[7] V. V. Shvartsman, W. Kleemann, R. Haumont and J. Kreisel, Large bulk polarization and regular domain structure in ceramic $BiFeO_3$, *Appl. Phys. Lett.* **90**, 172115 (2007).

[8] J. Wu, Z. Fan, D. Xiao, J. Zhu and J. Wang, Multiferroic bismuth ferrite-based materials for multifunctional applications: Ceramic bulks, thin films and nanostructures, *Progr. Mater. Sci.* **84**, 335 (2016).

[9] Y. Shuai, X. Ou, C. Wu, W. Zhang, S. Zhou, D. Bürger, H. Reuther, S. Slesazeck, T. Mikolajick, M. Helm and H. Schmidt, Substrate effect on the resistive switching in $BiFeO_3$ thin films, *J. Appl. Phys.* **111**, 07D906 (2012).

[10] R. Palai, R. S. Katiyar, H. Schmid, P. Tissot, S. J. Clark, J. Robertson, S. A. T. Redfern, G. Catalan and J. F. Scott, β phase and γ-β metal-insulator transition in multiferroic $BiFeO_3$, *Phys. Rev. B* **77**, 014110 (2008).

[11] R. Moubah, G. Schmerber, O Rousseau, D. Colson and M. Viret, Photoluminescence investigation of defects and optical band gap in multiferroic $BiFeO_3$ single crystals, *Appl. Phys. Exp.* **5**, 035802 (2012).

[12] N. I.Ilić, A. S. Džunuzović, J. D. Bobić, Bojan S. Stojadinović, P. Hammer, M. M. Vijatović Petrović, Z. D. Dohčević-Mitrović and B. D. Stojanović, Structure and properties of chemically synthesized $BiFeO_3$. Influence of fuel and complexing agent, *Ceram. Int.* **41**, 69 (2015).

[13] C. Ederer and N. A. Spaldin, Influence of strain and oxygen vacancies on the magnetoelectric properties of multiferroic bismuth ferrite, *Phys. Rev. B* **71**, 1 (2005).

[14] T. Gao, Z. Chen, F. Niu, D. Zhou, Q. Huang, Y. Zhu, L.Qin, X. Sun and Y. Huang, Shape-controlled preparation of bismuth ferrite by hydrothermal method and their visible-light degradation properties, *J. Alloys Compd.* **648**, 564 (2015).

[15] G. Geneste, Ch. Paillard and B. Dkhil, Polarons, vacancies, vacancy associations, and defect states in multiferroic $BiFeO_3$, *Phys. Rev. B* **99**, 024104 (2019).

[16] T. Tchelidze, T. Gagnidze and A. Shengelaya, Thermodynamic analysis of defect formation in $BiFeO_3$, *Phys. Stat. Solidi C* **12**, 117 (2015).

[17] X. Qi, J. Dho, R. Tomov, M. G. Blamire and J. L. MacManus-Driscoll, Greatly reduced leakage current and conduction mechanism in aliovalent-ion-doped $BiFeO_3$, *Appl. Phys. Lett.* **86**, 062903 (2005).

[18] G. D. Hu, S. H. Fan, C. H. Yang and W. B. Wu, Low leakage current and enhanced ferroelectric properties of Ti and Zn codoped $BiFeO_3$ thin film, *Appl. Phys. Lett.* **92**, 192905 (2008).

[19] H. Yang, Y. Q. Wang, H. Wang and Q. X. Jia, Oxygen concentration and its effect on the leakage current in $BiFeO_3$ thin films, *Appl. Phys. Lett.* **96**, 012909 (2010).

[20] Y. Wang and J. Wang, Modulated charged defects and conduction behaviour in doped $BiFeO_3$, *J. Phys. D: Appl. Phys.* **42**, 162001 (2009).

[21] E. Markiewicz, B. Hilczer, M. Błaszyk, A. Pietraszko and E. Talik, Dielectric properties of BiFeO3 ceramics obtained from mechanochemically synthesized nanopowders, *J. Electroceram.* **27**, 154 (2011).

[22] Sh. Ke, P. Lin, X Zeng, H. Huang, L. M. Zhou and Y.-W. Mai, Tuning of dielectric and ferroelectric properties in single phase $BiFeO_3$ ceramics with controlled Fe^{2+}/Fe^{3+} ratio, *Ceram. Int.* **40**, 5263 (2014).

[23] J. Moreau, C. Michel, R. Gerson and W. James, Ferroelectric $BiFeO_3$ X-ray and neutron diffraction study, *J. Phys. Chem. Solids* **32**, 1315 (1971).

[24] S. Mukherjee, A. Srivastava, R. Gupta and A. Garg, Suppression of grain boundary relaxation in Zr-doped $BiFeO_3$ thin films, *J. Appl. Phys.* **115**, 204102 (2014).

[25] A. K. Jonscher, *Dielectric Relaxation in Solids* (Chelsea Dielectrics, London, 1983).

[26] T. Wang, J. Hu, H. Yang, L. Jin, X. Wei, C. Li, F. Yan and Y. Lin, Dielectric relaxation and Maxwell-Wagner interface polarization in Nb_2O_5 doped $0.65BiFeO_3$-$0.35BaTiO_3$ ceramics, *J. App. Phys.* **121**, 084103 (2017).

[27] Y. Ma, X. M. Chen and Y. Q. Lin, Relaxor like dielectric behavior and weak ferromagnetism in $YFeO_3$ ceramics, *J. Appl. Phys.* **103**, 124111-1 (2008).

[28] C. Ang, Z. Yu and L. E. Cross, Oxygen-vacancy-related low frequency dielectric relaxation and electrical conduction in $Bi:SrTiO_3$, *Phys. Rev. B* **62**, 228 (2000).

[29] G. Gregori, R. Merkle and J. Maier, Ion conduction and redistribution at grain boundaries in oxide systems, *Progr. Mater. Sci.* **89**, 252 (2017).

[30] S. Kim and J. Maier, On the conductivity mechanism of nanocrystalline ceria, *J. Electrochem. Soc.* **149**, J73 (2002).

[31] H. Matsuoa, Y. Kitanaka, Y. Noguchi and M. Miyayama, Electrical conduction mechanism in $BiFeO_3$-based ferroelectric thin-film capacitors: Impact of Mn doping, *J. Asian Ceram. Soc.* **3**, 426 (2015).

[32] R. Y. Zheng, C. H. Sim and J. Wangw, Effects of SRO buffer layer on multiferroic $BiFeO_3$ thin films, *J. Am. Ceram. Soc.* **91**, 3240 (2008).